Two-Phase Equilibrium in Individual Nanoparticles of Bi-Sn

C.T. SCHAMP and W.A. JESSER

When evaluating the path of phase transformations in systems with nanoscopic dimensions, one often relies on bulk phase diagrams for guidance because of the lack of phase diagrams that show the effect of size. In order to provide insight into how phase diagrams can vary when a high surface curvature exists, binary alloys of Bi and Sn were investigated as a collection of individual crystalline particles vapor deposited onto amorphous carbon substrates in ultra-high vacuum. These crystallites were annealed after deposition to equilibrate the phases and structures. After annealing, they were transferred to the transmission electron microscope for analysis of the phase state as a function of composition and surface curvature, *i.e.,* particle radius. Individual crystallites were analyzed with respect to crystallinity, two-phase or one-phase coexistence, and composition. The data show that there is a critical size below which there is no limit to the solubility, in strong contrast to that found in the bulk system, which is a simple eutectic alloy with less than 0.3 pct solubility on the bismuth-rich solid solution side of the phase diagram and about 15 pct on the tin-rich side. The change in solubility limit with size was found to be equally strong in both the tin-rich terminal solid solution and the bismuth-rich terminal solid solution. A thermodynamic approach to using free-energy expressions modified to account for surface curvature can be successful in showing the shift in solubility with size. It is shown that the appropriate thermodynamic potential to minimize is a modified Helmholtz free energy.

I. INTRODUCTION

SIZE-DEPENDENT thermodynamic properties that are induced by strong capillarity forces on materials have been observed for many years. Depression of the melting temperature as a function of particle curvature (inverse radius) was first suggested theoretically about 100 years ago,[1] and experimentally shown over 50 years ago.[2] There have been relatively few studies looking into the effects of curvature on alloy systems,[3–6] and nearly all have involved the melting temperature depression. To date, the authors are aware of only three experimental studies of the size dependence of solid solubility and all show an enhancement with increasing surface cur-vature.[6,7,8] In the present article, solid solubility in isolated nanoparticles is studied and a three-dimensional *T-X* phase diagram is developed with the third axis of reciprocal radius (*i.e.,* particle curvature). Growth conditions, analysis, and a potential theoretical framework for the study of the equilibrium solid solubility of two-phase BiSn nanoparticles are described.

II. EXPERIMENTAL DETAILS

A PHI ultra-high vacuum system was modified to permit the simultaneous deposition of tin and bismuth. High-purity tin and bismuth are individually evaporated through resistive heating of isolated tungsten-wire baskets. The baskets are mounted on a four-pin electrical feedthrough, and isolated from one another by a molybdenum foil between the baskets to prevent cross-contamination. The substrates are standard 3-mm 200 mesh Cu transmission electron microscopy (TEM) grids supporting amorphous carbon purchased from the Ted Pella Company (Redding, CA). Heating of the substrate block holding these TEM grids are four resistively heated tungsten coils positioned symmetrically around the substrate holder, which is heated to about 90 °C for deposition. Immediately after deposition, the samples were annealed for about 1 hour, which should be adequate to attain equilibrium.[9] A load lock was installed on the ultra-high vacuum chamber to facilitate quick sample loading and unloading. For greater detail, the reader may refer to the Master's thesis of Schamp.[10]

Characterization of the nanoparticles is accomplished with a JEOL* 2010FX field emission analytical electron microscope, with an Oxford energy-dispersive spectrometer. The NIST computer program Desktop Spectrum Analyzer was used to analyze the energy-dispersive X-ray (EDX) spectra. Bright-field micrographs, selected area electron diffraction patterns, and nanobeam electron diffraction patterns were recorded and analyzed.

Typically, a bulk standard is used to determine the Cliff–Lorimer factor for composition determination, but this would contribute effects from absorption and florescence. In this case of isolated nanoparticles, these effects can be neglected.[7] To determine the Cliff–Lorimer EDX calibration factor, spectra were obtained from large single-phase particles whose compositions were assumed to be given by the bulk phase diagram. Using this as the standard, the Cliff–Lorimer factor was obtained through a typical technique described in Reference 11.

III. RESULTS

Single- and two-phase nanoparticles of Bi and Sn with a range of compositions and sizes were grown on thin amorphous carbon TEM grids, as described previously. A bright-field TEM micrograph of a typical two-phase sample is

*JEOL is a trademark of Japan Electron Optics Ltd., Tokyo.

C.T. SCHAMP, Graduate Student, and W.A. JESSER, Professor, are with the Department of Materials Science and Engineering, University of Virginia, Charlottesville, VA 22904. Contact e-mail: cts2v@virginia.edu

This article is based on a presentation made in the symposium "Phase Transformations Within Small-Size Systems: Thermodynamics, Phase Equilibria and Kinetics," which occurred February 14–16, 2005, during the TMS Spring Meeting in San Francisco, CA, under the auspices of the ASMI/MPMD-Phase Transformations, EMPMD/SMD-Chemistry & Physics of Materials, and EMPMD-Nanomaterials Committees.

shown in Figure 1(a). As can be seen in Figure 1(a), there is a variety of particle sizes in the field of view, which is consistent with a modal size distribution of thermally evaporated metals.[12] Figure 1(b) is the selected area diffraction pattern of the area that includes 1(a). Many of the rings are indexed showing that the figure is composed of body-centered-tetragonal Sn, rhom-bahedral Bi, and some bioxide. This particular sample was first grown over 1 year ago and recently reanalyzed. For comparison, Figures 2(a) through (c) were obtained shortly after growth, with the only exposure of the

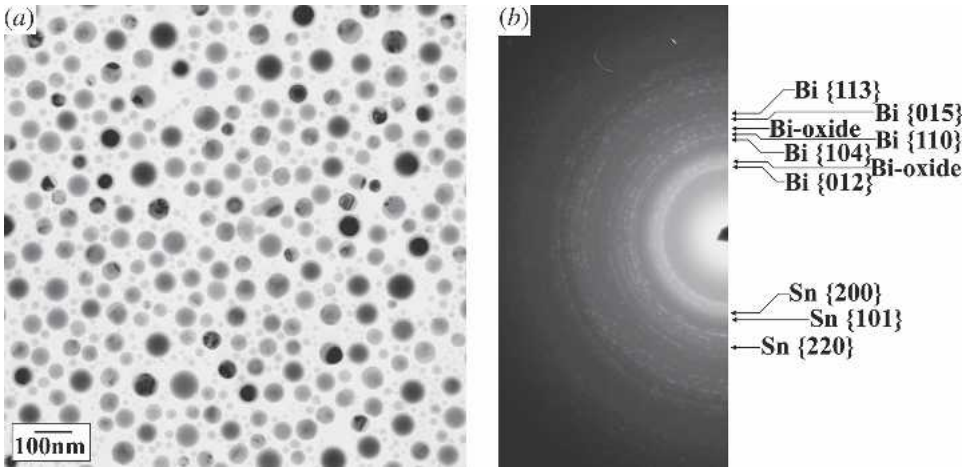

Fig. 1—(*a*) Bright-field micrograph of BiSn two-phase sample. (*b*) SAD pattern from (*a*) showing the existence of a bismuth rhombohedral phase, a tin body-centered-tetragonal phase, and the presence of bismuth oxide.

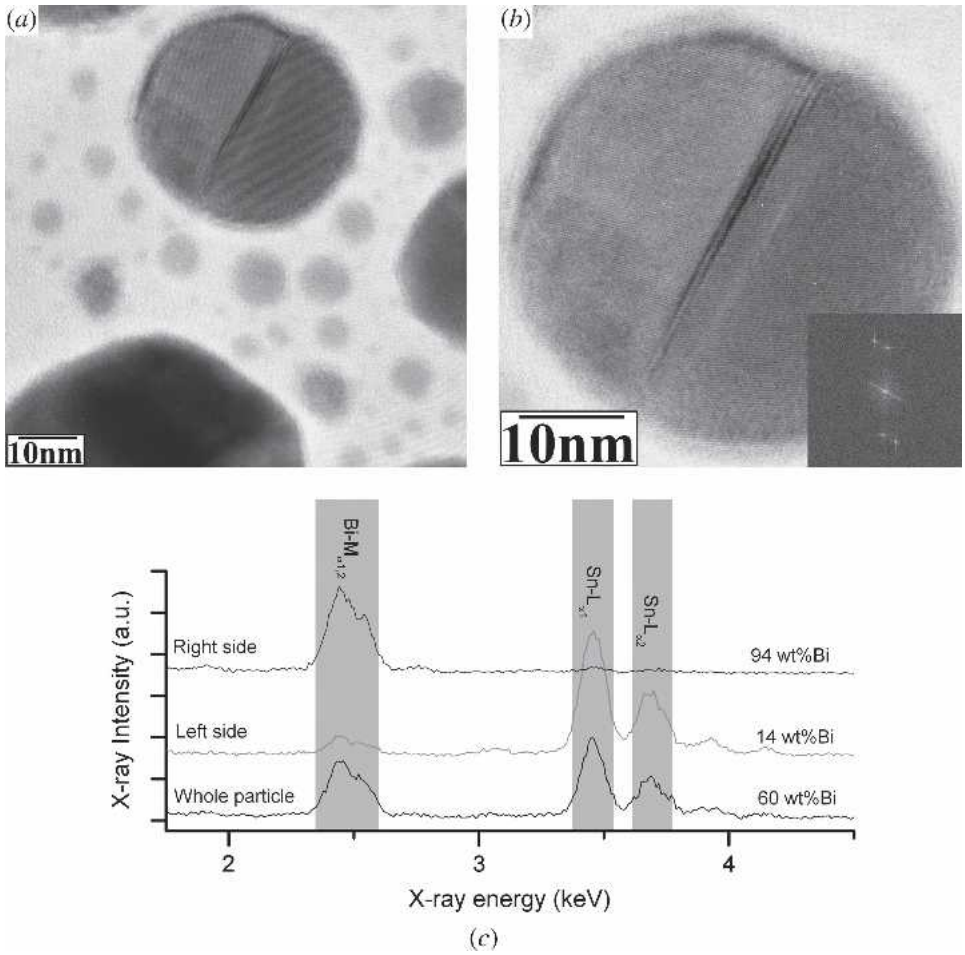

Fig. 2—(*a*) Bright-field micrograph showing single-phase and two-phase BiSn particles. (*b*) Magnified image of two-phase particle of (*a*) showing Moiré fringes in the tilted phase boundary. Inset is the digital diffractogram of the particle indicating the fringes are of the Sn {200} type and Bi {110} type. (*c*) EDX spectra of the particle in (*b*) from the right side, left side, and whole particle indicating the compositions are 94, 14, and 60 wt pct Bi, respectively.

sample to air being the several minutes that it took to transport the sample from the growth chamber to the TEM.

Figure 2(a) is another bright-field micrograph, similar to 1(a). The large two-phase particle shown in Figure 2(a) is further magnified and shown in Figure 2(b). The tapered line through the center of the particle is the phase boundary. The phase boundary is not perfectly parallel to the electron beam, resulting in the projected image of the phase boundary being extended and showing Moiré fringes. The inset in Figure 2(b) is the digital diffractogram of the nanoparticle, indicating that the lattice fringes imaged on the left-hand side of the particle are body-centered-tetragonal {200} Sn type and those on the right-hand side are {110} rhombohedral Bi type. Unfortunately, no two-phase particle was imaged showing two sets of lattice fringes in both phases, so an orientation relationship could not be determined.

Figure 2(c) shows EDX spectra from the right side, left side, and the whole of the particle in Figure 2(b). The Bi $M_{\alpha 1,2}$, Sn $L_{\alpha 1}$, and Sn $L_{\alpha 2}$ peaks are highlighted. The Bi $M_{\alpha 1,2}$ peak area is ratioed to the sum of the Sn $L_{\alpha 1}$ and Sn $L_{\alpha 2}$ peak areas through the Cliff–Lorimer equation to determine the compositions. This particular particle was found to have an overall composition of 60 wt pct Bi with the individual phases having compositions of 94 and 14 wt pct Bi.

For each two-phase particle, one X-ray spectrum was obtained from each of the phases and the particle as a whole. For single-phase particles, only one X-ray spectrum was acquired. During EDX spectra acquisition of the single-phase particles, the beam was expanded to just larger than the particle. For the two-phase particles, either EDX spectra were obtained with the beam expanded to less than the size of the smaller phase and periodically checked to ensure that the sample did not drift under the beam, or the EDX spectra were obtained while in diffraction mode with the beam fully converged. When viewing a convergent beam electron diffraction (CBED) pattern, it is easy to see when the sample drifts, because reflections from the second phase come into view. This is facilitated when few reflections are present in the case of a nonzone axis orientation, where one only needs to monitor the few reflections that originate from the phase of interest. If the sample drifts, the electron beam can be repositioned.

With similarly collected data from a number of particles, one can construct a map of regions of existence of two-phase fields and single-phase fields as a function of size and composition for a fixed temperature (in this case, room temperature). Such an isothermal section of a size-dependent phase diagram with axes of $1/r$ and composition was assembled and is shown as Figure 3.

In Figure 3, two-phase particles containing phase boundaries are represented by downward and upward pointing triangles, respectively, showing the Bi-poor (*i.e.,* Sn-rich) and Bi-rich phases in the coexisting two-phase particles. The average composition of these two-phase particles is denoted by circles with x's. Separating the two-phase region from the one-phase region is a solid line suggesting where the solvus boundary might lie.

Nearly all of the data were collected at room temperature, but to give an indication of the temperature dependence of the plot, a liquid nitrogen TEM cold stage was used to acquire several data points in the same manner as that

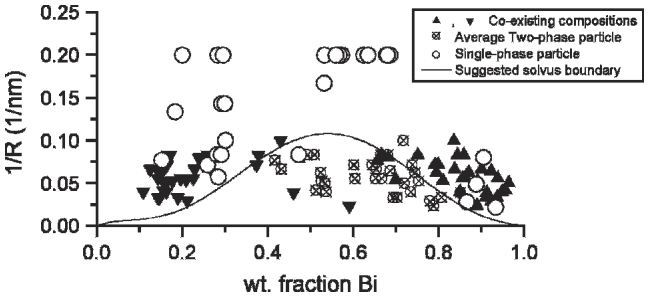

Fig. 3—Isothermal section at room temperature showing the size dependence of the BiSn phase diagram.

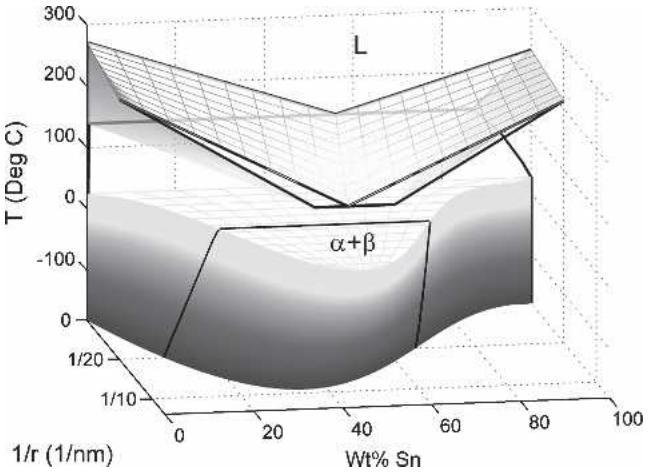

Fig. 4—Three-dimensional size-dependent phase diagram. The portion at temperatures greater than the eutectic temperature come from Reference 5. The portion with temperatures less than the eutectic temperature are from the current study. Thick dark lines represent *T-X* isopleths at $1/r = 0$ (bulk phase diagram) and at $1/r = 1/20$ nm. Each surface represents a boundary between one-phase regions and two-phase regions.

obtained at room temperature. While it is unlikely that the particles equilibrated at the liquid nitrogen temperature, the data are included to draw a three-dimensional *T*-1/*r*-*X* plot. These data and previous data from this lab[4,5] for the liquid-solid equilibrium of BiSn are used to construct a more complete phase diagram (Figure 4). The bulk *T-X* phase diagram is drawn at $1/R = 0$ and a second *T-X* phase diagram is drawn at $1/R = 1/20$ nm. Absent from this diagram is the three-phase equilibrium region.

IV. DISCUSSION

In considering which thermodynamic potential is appropriate to describe the observed equilibrium in two-phase nanoparticles, one must specify the character of the external wall enclosing the nanoparticle (system) and separating it from its surroundings (reservoir). Through the external wall, the system interacts with its reservoir. The appropriate wall character chosen was one that is impermeable, flexible, and diathermal. This is equivalent to having a closed system in contact with a pressure and a heat reservoir. The thermodynamic potential, which is a minimum for this case, has been shown to be

$$\phi = A_{\text{sys}} + P^{ex} V_{\text{sys}} \qquad [1]$$

where A_{sys} is the Helmholtz-free energy of the system. Equation [1] can be written for incompressible phases as

$$\phi^{\alpha\beta} = \sum_i n_i^{\alpha}\mu_i^{\alpha} + \sum\left(n_i^{\beta} + \Gamma_i^{\alpha\beta}\sum^{\alpha\beta} + \Gamma_i^{\beta g}\sum^{\beta g}\right)\mu_i^{\beta} + \gamma^{\alpha\beta}\sum^{\alpha\beta} + \gamma^{\beta g}\sum^{\beta g} + P^{ex}V_{sys} \quad [2]$$

where n is the number of atoms of component i, μ is the chemical potential of component i, Γ is the surface excess quantity of atoms of component i, Σ is the surface area, r is the interfacial energy, P^{ex} is the external pressure on the system, and V_{sys} is the total volume of the system.[13] The superscripts denote, respectively, the α phase, β phase, and surrounding gas phase g, whose function is to maintain the constant external pressure P^{ex}.

The potential ϕ is a Helmholz-free energy modified by the term $P^{ex}V_{sys}$ and shows the effect of the surface explicitly through the terms shown in Eq. [2] and implicitly in the capillarity effect, which increases the internal pressure of the phases through the equation

$$\Delta P = \frac{2f}{r} \quad [3]$$

Here, ΔP is the pressure increase induced by a curved surface of surface stress f and radius of curvature r. It is the elevated pressures in the system that change the chemical potentials of Eq. [2] and alter the equilibrium state from that of bulk phases to that of the nanoparticle system. Earlier experimental work on the depression of melting temperature in nanoparticles showed that a larger melting depression occurred when the particles were spheres with a high surface curvature than when the particles were disc shaped with a higher surface-to-volume ratio.[13] This result is consistent with the idea that it is the surface curvature that is important in Eq. [2], not simply the surface-to-volume ratio shown explicitly by the surface terms of that equation. However, there are situations for which the amount of area dominates the curvature effect. Such cases occur when the surface/interface atoms are attracted to or repelled from the area. In this case, the atom excess or deficiency will primarily be proportional to the total area.

The values of composition and phase fraction that correspond to minima in the Helmholtz free-energy expression as a function of size of the nanoparticle allows one to determine the phase diagram as a function of particle size. This has been performed for the case of Pb-Bi.[14] Here, the significant features of the phase diagram for nanoparticles are reviewed qualitatively. These features are as follows. (1) Two-phase fields pinch off to a line seemingly in violation of the Gibbs phase rule but not so because of the pressure dependence on size as an additional variable, (2) Immiscible systems in bulk can become completely miscible when the size of the nanoparticle becomes 10 nm or less. This is an example of a two-phase field pinching off as a function of size and is illustrated in Figures 3 and 4, (3) The transition temperatures, *e.g.*, melting temperature and eutectic temperature, are significantly displaced from bulk values, and (4) The crossing from a two-phase field into a one-phase field and similarly the reverse transition is observed to occur discontinuously as a function of temperature.[5] The consequence of this is that the construction of tie lines becomes altered from the procedure for bulk phase diagrams in that their ends lie outside the two-phase field and map into bands of some width in the one-phase fields on either side of the two-phase field.

Concept 4, which emerged from the thermodynamic model, was used in Figure 3 to draw a suggested solvus boundary as the limit to the region in which two phases coexist in equilibrium. The boundaries are also drawn in Figure 4 as such limits. In addition to these boundaries, pairs of triangles are shown in Figure 3 representing the compositions of each of the two ends of the tie-lines, *i.e.*, denoting the respective equilibrium compositions of each of the two phases in contact across their interface. These tie-line ends (triangles) are seen to lie in bands on either side of the two-phase field. It is noteworthy that the single-phase data points (open circles) fall within these bands. This feature is consistent with the bands representing the ends of the tie-lines being detached from the two-phase field. Each band (tie-line end) lies in one of the two one-phase fields on either side of the two-phase field.

The x-filled circles in Figure 3 indicate the average composition of the two-phase particles and should therefore fall only within the two-phase field. The suggested solvus boundary is drawn reflecting the positions of most of the data points. Several single-phase data points lie within the two-phase region. These data points could be considered to be an inaccurate measurement, but no errors were found in any of the analysis, and are included for completeness even though they do not conform to the ideal phase diagram for nanoparticles. Figure 3 is believed to be a confirmation of the preceding qualitative point (4), that the result in detached tie-line ends from the two-phase coexistence region bounded by its solvus boundaries. It also stands as an example of point (2).

V. CONCLUSIONS

In the Sn-Bi system, the solid solubility is enhanced with increasing curvature, to the extent that total miscibility is achieved for curvatures greater than about 0.1 nm^{-1}.

In isolated nanoparticles, the solubility of Sn in Bi is greatly enhanced, contrary to the bulk phase diagram in which Sn has nearly no solubility in Bi. The surface curvature therefore can be interpreted as a solubility parameter for equilibrated isolated nanoparticles. This feature raises caution when using bulk phase diagrams to infer the temperature behavior of phase fields in nanoparticles.

VI. ACKNOWLEDGMENTS

The authors gratefully acknowledge the support of the United States-Israeli Binational Science Foundation, under Grant No. 96-00027/2; the University of Virginia for the Academic Enhancement, under Grant No. 1-98881; and the MRSEC Center for Nanoscopic Materials Design by the National Science Foundation under Award No. DMR-0080016.

REFERENCES

1. P. Pawlow: *Z. Phys. Chem.,* 1909, vol. 65, pp. 545-48.
2. M. Takagi: *J. Phys. Soc. Jpn.,* 1954, vol. 9, pp. 359-63.
3. R.P. Berman: Ph.D. Thesis, Simon Fraser University, 1976.

4. G.L. Allen and W.A. Jesser: *J. Cryst. Growth,* 1984, vol. 70, pp. 546-51.
5. W.A. Jesser, G.J. Shiflet, G.L. Allen, and J.L. Crawford: *Mater. Res. Innovation,* 1999, vol. 2, pp. 211-16.
6. L.S. Palatnik and B.T. Boiko: *Phys. Met. Metallogr.,* 1961, vol. 11, pp. 119–23.
7. C.E. Lyman, R.E. Lakis, H.G. Stenger, B. Totdal, and R. Prestvik: *Mikrochim. Acta,* 2000, vol. 132 (2–4), pp. 301-08.
8. H. Yasuda and H. Mori: *J. Cryst. Growth,* 2002, vol. 237, pp. 234-38.
9. H. Yasuda and H. Mori: *Phys. Rev. Lett.,* 1992, vol. 69 (26), pp. 3747-50.
10. C.T. Schamp: Master's Thesis, University of Virginia, Charlottesville, VA, 2001.
11. D.B. Williams and C.B. Carter: *Transmission Electron Microscopy: A Textbook for Materials Science,* Plenum Press, New York, NY, 1996.
12. R.A. Bennett, D.M. Tarr, and P.A. Mulheran: *J. Phys.: Condens. Mater.,* 2003, vol. 15, pp. S3139-52.
13. R.A. Bayles: Ph.D. Thesis, University of Virginia, Charlottesville, VA, 1979.
14. W.A. Jesser, R.Z. Shneck, and W.W. Gile: *Phys. Rev. B: Condens. Matter,* 2004, vol. 69 (14), pp. 1441-21.